PCCP

RSC Publishing

Infrared spectrum of the disilane cation (Si$_2$H$_6$$^+$) from Ar-tagging spectroscopy

Marco Savoca, Martin Andreas Robert George, Judith Langer and Otto Dopfer*

The infrared spectrum of the disilane cation, Si$_2$H$_6$$^+$, in its ^{2}A$_{1g}$ ground state is inferred from photodissociation of cold Si$_2$H$_6$$^+$–Ar$_n$ complexes (n = 1, 2). Vibrational analysis is consistent with a D_{3d} symmetric structure of H$_3$SiSiH$_3$$^+$ generated by ionization from the bonding σ$_{SiSi}$ orbital. Structural, vibrational, and electronic properties of Si$_2$H$_6$$^{(+)}$ and Si$_2$H$_6$$^+$–Ar$_{1,2}$ are determined at the MP2/aug-cc-pVTZ and B3LYP/aug-cc-pVTZ levels. Ar ligands bind weakly at the C_3 axis on opposite sides to Si$_2$H$_6$$^+$ with only a minor impact on the Si$_2$H$_6$$^+$ properties. The calculations reveal a low-energy H$_2$SiHSiH$_3$$^+$ isomer with C_s symmetry and a Si–H–Si bridge, which is only ∼15 kJ mol^{-1} above the D_{3d} structure.

1. Introduction

Although Si and C are both group IV elements, their bonding characteristics are substantially different. As a result of the much weaker and less directional Si–Si bonds, Si-containing molecules exhibit a larger variety of binding motifs as compared to the corresponding C-bearing species. For example, Si$_x$H$_y$ molecules often exhibit Si–H–Si bridges,[1–3] which are quite rare for C$_x$H$_y$. In contrast to the well-characterized C$_x$H$_y$ molecules, considerably less information is available for the more reactive and less stable Si$_x$H$_y$ analogues, because precursors for the latter are less readily available. For example, although IR spectra are available for SiH$_y$$^+$ with y = 3, 5, and 7,[4–6] no vibrational and electronic spectra are available for Si$_x$H$_y$$^+$ cations with $x \geq 2$. Characterization of Si$_x$H$_y$ and their ionic species is not only motivated from fundamental aspects in the theory of chemical bonding but also from understanding of processes in (di)silane plasmas[2,7] and interstellar media.[3,8] In addition, hydrogen passivation of the highly reactive bare silicon clusters and cages has been suggested as a possible route to generate novel stable silicon nanostructures with potential applications in materials science.[9,10] To this end, we set up a program to systematically characterize the geometric and electronic structure of Si$_x$H$_y$ molecules, their ions, and their clusters by spectroscopy and quantum chemical calculations. Herein we report infrared (IR) spectra of Ar clusters of the disilane cation (Si$_2$H$_6$$^+$) obtained by IR photodissociation (IRPD) spectroscopy of mass selected Si$_2$H$_6$$^+$–Ar$_n$ clusters, which have been synthesized in a supersonic plasma expansion of SiH$_4$. This tagging approach[11,12] has

previously been employed to investigate a variety of fundamental C$_x$H$_y$$^+$ ions, including CH$_3$$^+$,[13–15] C$_2H_2$$^+$,[16,17] C$_2H_3$$^+$,[18] C$_3H_3$$^+$,[19–23] C$_3H_5$$^+$,[24] C$_6H_5$$_{-7}$$^+$,[25–34] and C$_{10}H_{16}$$^+$,[35] as well as SiOH$^+$ cluster ions,[36,37] but seems to be applied for the first time to Si$_x$H$_y$$^+$ ions.

Neutral Si$_2$H$_6$ is a well-characterized molecule. It has a staggered equilibrium structure with D_{3d} symmetry in its ^{1}A$_{1g}$ ground electronic state (Fig. 1). All fundamental vibrational frequencies are accurately known from IR and Raman spectroscopy.[38–41] The geometric parameters of Si$_2$H$_6$ have been determined by electron diffraction to be R = 2.331(3) Å, r = 1.493(3) Å, and θ = 110.3(4)°.[42] The threefold barrier for internal rotation *via* the transition state (TS) with D_{3h} symmetry has been determined from high-resolution torsional and tunnelling spectroscopy of IR transitions to be V_3 = 407 cm^{-1}.[40,41] The 12 vibrational fundamentals of Si$_2$H$_6$, ν_{1-12}, transform in D_{3d} as Γ_{vib} = 3a$_{1g}$ + a$_{1u}$ + 2a$_{2u}$ + 3e$_u$ + 3e$_g$. We follow the notation of vibrational modes given previously in ref. 38 and 39. The fundamentals with a$_{2u}$ ($\nu_{5/6}$) and e$_u$ (ν_{7-9}) symmetry are IR active, whereas those with a$_{1g}$ (ν_{1-3}) and e$_g$ (ν_{10-12}) are Raman active.

In contrast to neutral Si$_2$H$_6$, surprisingly little spectroscopic and quantum chemical data are available for the corresponding Si$_2$H$_6$$^+$ cation and its clusters, probably due to the experimental challenges involved in preparing sufficient number densities of cold (cluster) ions. The limited number of relatively low-level quantum chemical calculations predicts that adiabatic ionization of Si$_2$H$_6$ occurs from the bonding σ$_{Si–Si}$ orbital with a$_{1g}$ symmetry, leading to a ^{2}A$_{1g}$ ground electronic state with staggered configuration (D_{3d}).[1,43] As a consequence of ionization to the ionic ground state, the Si–Si bond contracts substantially and the SiSiH bond angle strongly decreases, while the Si–H bond length is less affected. The corresponding values obtained at the MP2/6-31G* level are reported as ΔR = +0.32 Å, $\Delta\theta$ = −12°, and Δr = −0.016 Å, respectively.[1]

Institut für Optik und Atomare Physik, Technische Universität Berlin, Hardenbergstraße 36, 10623 Berlin, Germany. E-mail: dopfer@physik.tu-berlin.de
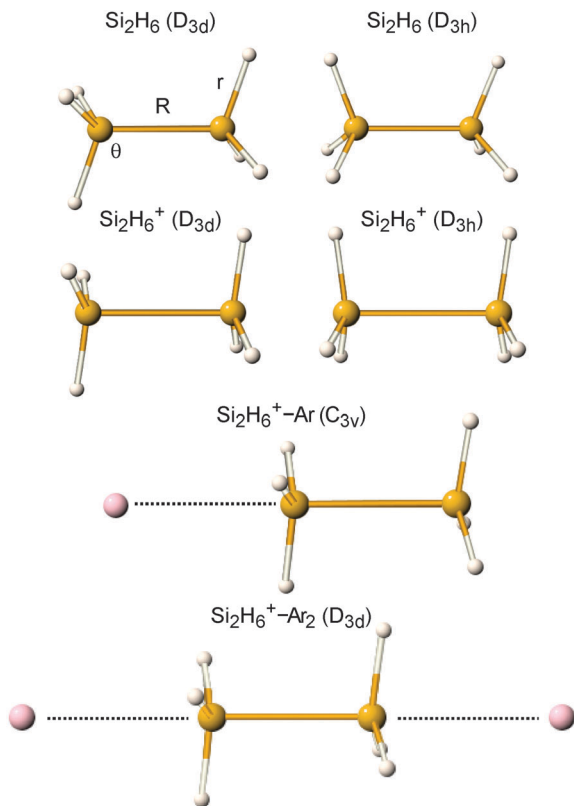
Fig. 1 Calculated equilibrium structures of Si_2H_6 and $Si_2H_6^+$ with D_{3d} and D_{3h} symmetry in their ground electronic states obtained at the B3LYP/aug-cc-pVTZ level. Minimum structures of $Si_2H_6^+$–Ar_n with $n = 1$ and 2 are given as well. Corresponding geometrical, vibrational, and energetic parameters are listed in Tables 1 and 2.

As a result of the large geometry change upon ionization and the induced long Franck–Condon progressions in the totally symmetric SiH_3 umbrella and low-frequency Si–Si stretch modes, the He(I) photoelectron spectrum of Si_2H_6 is broad (>1 eV) and essentially unresolved at the achieved spectral resolution (~ 200 cm^{-1}), largely preventing vibrational characterization of the cation ground state.[44,45] The only vibrationally resolved feature that has been assigned to the symmetric SiH_3 umbrella mode is $\nu_2(a_{1g}) \sim 0.11$ eV (~ 900 cm^{-1}).[45,46] Photoionization mass spectrometry of Si_2H_6 yields an adiabatic ionization potential of AIE = 9.74(2) eV, and low appearance energies of $\leq 10.04(2)$ and $\leq 10.81(2)$ eV for H_2 elimination generating $H_2SiSiH_2^+$ and $HSiSiH_3^+$, respectively.[46]

Here we report IRPD spectra and quantum chemical calculations of $Si_2H_6^+$–Ar_n clusters with $n = 1$ and 2. The major motivation for this work resulted from the following aspects. (1) The IRPD spectra of cold $Si_2H_6^+$–Ar_n clusters provide the first IR vibrational signatures of the fundamental $Si_2H_6^+$ cation. (2) Neither spectroscopic nor computational data are available for clusters of $Si_2H_6^+$. Hence, this study on $Si_2H_6^+$–Ar_n provides a first impression of the intermolecular interaction of the $Si_2H_6^+$ cation with neutral ligands. (3) Ab initio and density functional calculations are performed for $Si_2H_6^+$–Ar_n at the MP2 and B3LYP levels using the aug-cc-pVTZ basis set. Thus, these

calculations employ a much higher theoretical level as compared to previous quantum chemical studies. For example, geometry optimization for $Si_2H_6^+$ has only been reported up to the MP2/6-31G* level. The major issues addressed in this work are the effects of ionization and Ar complexation on the geometrical, vibrational, and electronic properties of disilane. We also consider the potential for SiH_3 internal rotation because no information appears to exist for the barrier in the ionic ground state. In addition, we explored $Si_2H_6^+$ structures with connectivities other than $H_3SiSiH_3^+$ and report for the first time a low-energy isomer of the disilane cation with a $H_2SiHSiH_3^+$ structure featuring a Si–H–Si bridge.

2. Experimental and computational techniques

IRPD spectra of $Si_2H_6^+$–Ar_n with $n = 1$ and 2 are obtained in a tandem quadrupole mass spectrometer coupled to an electron impact ionization source and an octopole ion trap.[47,48] Weakly-bound $Si_xH_y^+$–Ar_n clusters are generated in a pulsed supersonic plasma expansion by electron impact and chemical ionization of a suitable gas mixture of SiH_4 and Ar close to the nozzle orifice and subsequent clustering reactions in the high pressure regime of the expansion. A typical mass spectrum of the ion source obtained for expanding a SiH_4/He/Ar mixture with a ratio of 1/20/200 at 5 bar stagnation pressure is shown in Fig. 2. The major cluster series observed are Ar_n^+, $Si_xH_y^+$–Ar_n, $Si_xH_y^+$–$(SiH_4)_n$, and $Si_xH_y^+$–$(SiH_4)_n$–Ar_m. Significant polymerization reactions are observed up to $Si_xH_y^+$ with $x = 3$. In general, the abundance of $Si_xH_y^+$–Ar_n clusters decreases rapidly with increasing cluster size n, consistent with the formation of weakly-bound clusters by sequential addition of individual ligands to the molecular $Si_xH_y^+$ ion. Although the abundance of $Si_2H_6^+$ is at least one order lower compared to the most abundant $Si_xH_y^+$ ions (SiH_3^+ and $Si_2H_7^+$), respectable IRPD spectra could be recorded for its weakly-bound $Si_xH_y^+$–Ar_n clusters with $n = 1$ and 2, illustrating the high sensitivity of the experimental approach. $Si_2H_6^+$–Ar_n ions of interest are mass selected by the first quadrupole and

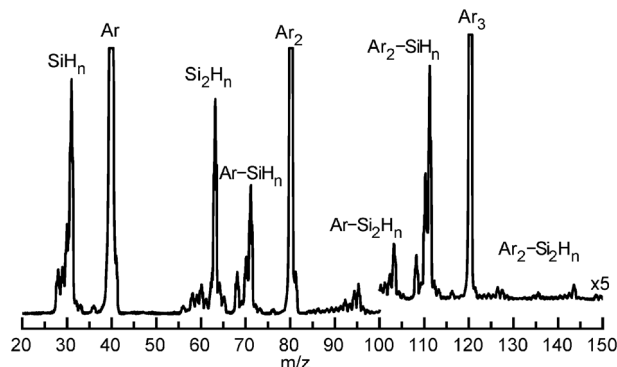**Fig. 2** Typical mass spectrum of the electron impact cluster ion source for an SiH_4/He/Ar expansion (1/20/200) at 5 bar stagnation pressure. Major cluster series observed are Ar_n^+, $Si_xH_y^+$–Ar_n, $Si_xH_y^+$–$(SiH_4)_n$, and $Si_xH_y^+$–$(SiH_4)_n$–Ar_m. Part of the spectrum is vertically expanded by a factor of 5.

irradiated in an adjacent octopole with tuneable IR laser radiation generated by an IR optical parametric oscillator pumped by a Q-switched nanosecond Nd:YAG laser. The IR laser is characterized by a pulse energy of ~ 0.1–0.5 mJ in the 650–2200 cm^{-1} range, a repetition rate of 10 Hz, and a bandwidth of 1 cm^{-1}. Calibration of the IR laser frequency is accomplished by a wavemeter. Resonant vibrational excitation of $Si_2H_6^+$–Ar_n induces evaporation of a single Ar ligand (Ar-tagging), according to:

$$Si_2H_6^+\text{–}Ar_n + h\nu_{IR} \rightarrow Si_2H_6^+\text{–}Ar_m + (n - m)\,Ar \quad (m = n - 1) \tag{1}$$
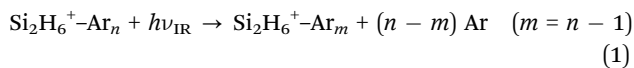
The resulting $Si_2H_6^+$–Ar_{n-1} fragment ions are selected by the second quadrupole and monitored as a function of the laser frequency to obtain the IR photodissociation spectrum of $Si_2H_6^+$–Ar_n. To separate the fragment ions arising from metastable decay and laser-induced dissociation, the ion source is triggered at twice the laser frequency, and signals from alternating triggers are subtracted. Although the IR spectra have been normalized for laser intensity fluctuations, the relative intensities of widely spaced bands are believed to be accurate to within a factor of two, mainly due to the changes in the spatial overlap between the ion and IR laser beams. As the mass spectrum of the ion source is rather complex, collision-induced dissociation (CID) experiments are performed to verify the composition of the mass-selected parent ions. To this end, the octopole is filled with N_2 collision gas up to 10^{-5} mbar, facilitating single collision conditions with a collision energy of 10 eV in the laboratory frame. The CID spectrum of mass-selected $Si_2H_6^+$–Ar_2 in Fig. 3 demonstrates Ar loss as only fragment channels, indicating that the composition of the m/z 142 ion is indeed 102$^+$-Ar or 62$^+$-Ar$_2$, consistent with the $Si_2H_6^+$–Ar_2 parent ion.

Si_2H_6, $Si_2H_6^+$, and $Si_2H_6^+$–Ar_n clusters are characterized in their ground electronic states by quantum chemical calculations at the B3LYP and MP2 levels using the cc-pVDZ and aug-cc-pVTZ basis sets,[49] to investigate the effects of ionization and Ar complexation on the geometric, vibrational, and electronic structure as well as the SiH_3 internal rotation potential. As the results using the two different basis sets are similar for the monomer species, only the data for the larger aug-cc-pVTZ basis set are reported here. All coordinates are relaxed for the search of stationary points on the potential, and their nature as minimum or transition state (TS) is established by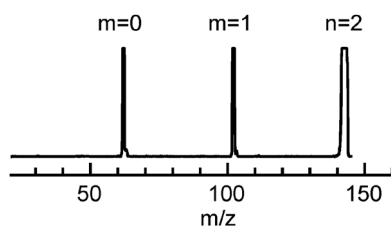 harmonic frequency analysis. Energies are corrected for harmonic zero-point vibrational energy. Harmonic frequencies are scaled by factors of 0.9780 (0.9518) and 0.9942 (0.9742) for B3LYP (MP2) frequencies above and below 1500 cm^{-1}, respectively, to optimize the agreement between the calculated and the measured frequencies of Si_2H_6. Such a dual scaling factor procedure accounts for the rather different anharmonicity of the Si–H hydride stretch modes and the other vibrations.[50] Application of these scaling factors to the B3LYP (MP2) harmonic frequencies could reproduce the measured frequencies of the fundamentals to better than 13 (18) cm^{-1}, with an average deviation of 5 (5) cm^{-1}. Spin contamination for the radical cation species is negligible, with values of < 0.006 and $< 10^{-4}$ for $\langle S^2 \rangle$ -0.75 before and after annihilation, respectively. The charge distribution is calculated using the natural bond orbital (NBO) population analysis.

3. Results and discussion

3.1 Experimental IR spectra

The IRPD spectra of $Si_2H_6^+$–Ar and $Si_2H_6^+$–Ar_2 recorded in the Ar loss channel are shown in Fig. 4. They exhibit only three transitions (A–C) in the investigated frequency range (650–2230 cm^{-1}), consistent with the high symmetry of the $Si_2H_6^+$ ion and the weak perturbation by the Ar ligands. The transitions A at 725 and 719 cm^{-1} for $n = 1$ and 2 are assigned to the antisymmetric linear combination of the umbrella inversion motions, ν_6. The bands B at 926 and 925 cm^{-1} for $n = 1$ and 2 are attributed to the asymmetric SiH_3 deformation mode, ν_8. While the assignments of A and B to fundamentals of $Si_2H_6^+$ are fully supported

Fig. 3 CID spectrum obtained by mass-selecting $Si_2H_6^+$–Ar_2 (m/z 142) with the first quadrupole and scanning the second quadrupole. The only fragments observed are $Si_2H_6^+$–Ar_m with $m = 0$ and 1 (m/z 62 and 102) indicating that the composition of the m/z 142 ion is indeed 62$^+$-Ar$_2$ or 102$^+$-Ar, consistent with $Si_2H_6^+$–Ar_2. All peaks are saturated in order to detect possible weak fragment signals.

Fig. 4 Experimental IRPD spectra of $Si_2H_6^+$–Ar and $Si_2H_6^+$–Ar_2 compared to linear IR absorption spectra of $Si_2H_6^+$–Ar (C_{3v}), $Si_2H_6^+$–Ar_2 (D_{3d}), $Si_2H_6^+$ (D_{3d}, D_{3h}), and Si_2H_6 (D_{3d}) calculated at the B3LYP/aug-cc-pVTZ level (Fig. 1 and Table 2). The calculated spectra are drawn to the same scale.

by the calculations presented below, the interpretation of bands **C** at 1500 and 1505 cm^{-1} for $n = 1$ and 2 is less clear, because $Si_2H_6^+$ does not have any fundamental mode in this frequency range. Currently, the tentative assignment is to the $\nu_6 + \nu_2$ combination band. The $Si_2H_6^+$–Ar$_2$ spectrum could only be obtained in the $Si_2H_6^+$–Ar fragment channel. The fact that no laser-induced dissociation signal was detected in the $Si_2H_6^+$ channel indicates that the IR photon energy of the observed IR resonances is insufficient to evaporate both Ar ligands. The widths of the vibrational transitions (5–25 cm^{-1}) result mainly from unresolved rotational fine structure.

Efforts in recording the IR(M)PD spectrum of $Si_2H_6^+$ monitored in the $Si_2H_4^+$ fragment channel failed despite the relatively low reported dissociation energy of < 0.3 eV (~ 2400 cm^{-1}). The lack of observation of resonant laser-induced dissociation is ascribed to the single-photon absorption conditions[48,51–53] in connection with the low IR photon energies (< 2200 cm^{-1}) and the high metastable decay background signal observed for H_2 elimination of internally hot ions generated in the ion source.

3.2 Computational results

The computational results obtained for Si_2H_6, $Si_2H_6^+$, and $Si_2H_6^+$–Ar$_n$ relevant for the present work are summarized in Fig. 1, 4, and 5 and Tables 1 and 2, respectively.

In agreement with experiment and previous computations, the global minimum of Si_2H_6 in its $^1A_{1g}$ ground electronic state obtained in the present B3LYP and MP2 calculations has a staggered equilibrium structure with D_{3d} symmetry (Fig. 1). The structural parameters of $R_e = 2.35$ Å, $r_e = 1.48$ Å, and $\theta_e = 110°$ agree well with the values derived from electron scattering, $R = 2.331(3)$ Å, $r = 1.493(3)$ Å, and $\theta = 110.3(4)°$.[42] The rotational constants of $A_e = 43\,104$ and $B_e = 5017$ MHz (B3LYP) are also close to the measured values of $A_0 = 43\,208(23)$ and $B_0 = 5120.095(45)$ MHz.[40] Similarly, the scaled fundamental frequencies can reproduce the measured fundamentals well, with a maximum uncertainty of less than 20 cm^{-1}. Since the B3LYP values are more accurate, we refer to these frequencies in the text and in Fig. 4, although Table 2 offers also the only slightly less accurate MP2 values. The simulated IR spectrum of Si_2H_6 in Fig. 4 shows all five IR active fundamentals
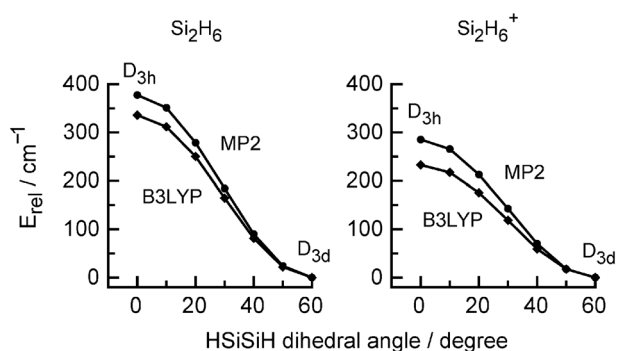

Fig. 5 Potential for internal SiH$_3$ rotation of Si_2H_6 and $Si_2H_6^+$ as a function of the HSiSiH dihedral angle evaluated at the MP2 and B3LYP levels using the aug-cc-pVTZ basis set. The staggered D_{3d} structure (60°) is more stable than the eclipsed D_{3h} geometry (0°) for both charge states.

Table 1 Geometrical parameters (in Å and degree), relative energies and binding energies (in cm^{-1}), and NBO charge distribution (in e) of the equilibrium structures of Si_2H_6, $Si_2H_6^+$, and $Si_2H_6^+$–Ar$_n$ with $n = 1$ and 2 evaluated at the MP2 and B3LYP levels using the aug-cc-pVTZ basis set (Fig. 1)

	$Si_2H_6{}^a$ D_{3d}	Si_2H_6 D_{3h} (TS)	$Si_2H_6^+{}^b$ D_{3d}	$Si_2H_6^+$ D_{3h} (TS)	$Si_2H_6^+$–Ar^c C_{3v}	$Si_2H_6^+$–Ar$_2$ D_{3d}
MP2						
$E_{rel}{}^d$	0	347 (351)	0	219 (273)		
D_0					881	815
R	2.3491	2.3601	2.7193	2.7512	2.7193	2.7168
r	1.4812	1.4806	1.4670	1.4667	1.4660* 1.4673	1.4664
θ	110.2	110.4	98.0	98.2	96.6* 98.6	97.3
$R_{Si–Ar}$					2.9931	3.0577
q_{Si}	0.597	0.596	0.991	0.974	0.973* 0.980	0.967
q_H	−0.199	−0.199	−0.158	−0.157	−0.165* −0.167	−0.168
q_{Ar}					0.043	0.036
B3LYP						
$E_{rel}{}^d$	0	335 (309)	0	232 (227)		
D_0					428	364
R	2.3537	2.3655	2.7426	2.7744	2.7451	2.7584
r	1.4858	1.4855	1.4721	1.4732	1.4715* 1.4731	1.4719
θ	110.4	110.6	98.0	98.2	96.8* 98.7	97.6
$R_{Si–Ar}$					3.1204	3.2183
q_{Si}	0.427	0.434	0.822	0.823	0.786* 0.814	0.789
q_H	−0.142	−0.145	−0.107	−0.107	−0.110* −0.107	−0.110
q_{Ar}					0.051	0.040

^{a} Experimental values are $R = 2.331(3)$ Å, $r = 1.493(3)$ Å, and $\theta = 110.3(4)°$.[42] ^{b} MP2/6-31G* values are $R = 2.659$ Å, $r = 1.487$ Å, and $\theta = 110.4°$.[1] ^{c} Values of the parameters related to the SiH$_3$ moiety binding to Ar are indicated by asterisks. ^{d} Numbers in parentheses include zero-point energy.

with a$_{2u}$ ($\nu_{5/6}$) and e$_u$ ($\nu_{7–9}$) symmetry. These include the two asymmetric Si–H stretch modes $\nu_{5/7}$, the asymmetric umbrella inversion mode ν_6, an asymmetric SiH$_3$ deformation mode ν_8, and an asymmetric SiH$_3$ rocking mode ν_9. The NBO charges of $q_{Si} = 0.6$ e and $q_H = -0.2$ e (MP2) are in line with the higher electronegativity of H. The potential for internal SiH$_3$ rotation of Si_2H_6 is shown in Fig. 5. The HSiSiH dihedral angle has been varied in steps of 10°, and for each angle all other coordinates have been relaxed. The threefold barrier occurs at the transition state with eclipsed configuration (0°, Fig. 1, D_{3h}) and amounts to $V_3 = 377$ and 336 cm^{-1} at the MP2 and B3LYP levels, respectively, in good agreement with the experimental value of $V_3 = 407$ cm^{-1}.[40,41] The geometrical and vibrational parameters of the D_{3h} transition state are quite similar to those of the D_{3d} minimum.

Similar to neutral Si_2H_6, the global minimum of $Si_2H_6^+$ in its $^2A_{1g}$ ground electronic state also has a staggered equilibrium structure with D_{3d} symmetry. The adiabatic ionization energies of AIE = 9.49 (9.56) eV calculated at the B3LYP (MP2) level are consistent with the experimental value of AIE = 9.74(2) eV,[46] indicating that the chosen computational approaches describe the electronic structure of Si_2H_6 well in both charge states.

Table 2 Experimental and calculated vibrational frequencies (in cm^{-1}) of Si$_2$H$_6$, Si$_2$H$_6^+$, and Si$_2$H$_6^+$–Ar$_n$ with n = 1 and 2 evaluated at the MP2 and B3LYP levels using the aug-cc-pVTZ basis set (Fig. 1)[a]

Mode[b]	Description[c]	Si$_2$H$_6$[d] D_{3d}	Si$_2$H$_6$ D_{3d}	Si$_2$H$_6^+$ D_{3d}	Si$_2$H$_6^+$ D_{3h} (TS)	Si$_2$H$_6^+$–Ar C_{3v}	Si$_2$H$_6^+$–Ar$_2$ D_{3d}
ν_1(a$_{1g}$)	σ_{Si-H}	2163	2161	2207	2209	2205 (0.2)	2208
			2161	2201	2197	2194 (0.5)	2201
ν_2(a$_{1g}$)	β_{SiH_3}	920	918	817	826	818 (3)	819
			917	787	797	787 (0.1)	784
ν_3(a$_{1g}$)	σ_{Si-Si}	432	430	233	234	237 (8)	243
			419	212	212	214 (5)	213
ν_4(a$_{1u}$)	τ_{SiH_3}	131.0	137	116	i113	118	119
			132	94	i93	109	103
ν_5(a$_{2u}$)	σ_{Si-H}	2154.3	2154 (118)	2206 (0.1)	2207 (0.2)	2210 (0.01)	2208 (0.3)
			2153 (116)	2198 (1)	2194 (0.7)	2201 (0.3)	2198 (0.05)
ν_6(a$_{2u}$)	β_{SiH_3}	843.5	843 (542)	741 (452)	742 (470)	737 (583)	732 (710)
			844 (507)	718 (360)	722 (371)	715 (461)	709 (554)
						725	719
ν_7(e$_u$)	σ_{Si-H}	2178.6	2172 (405)	2265 (20)	2267 (20)	2267 (18)	2267 (24)
			2173 (395)	2264 (15)	2260 (15)	2264 (14)	2265 (19)
ν_8(e$_u$)	β_{SiH_3}	939.6	953 (184)	917 (218)	917 (215)	915 (187)	910 (195)
			950 (162)	913 (195)	914 (191)	912 (171)	910 (176)
						926	925
ν_9(e$_u$)	γ_{SiH_3}	379.3	362 (46)	246 (0.5)	307 (1)	293 (1)	356 (1)
			370 (41)	254 (0.1)	307 (0.2)	285 (0.2)	403 (0.02)
ν_{10}(e$_g$)	σ_{Si-H}	2155?	2164	2260	2260	2259 (5)	2260
			2163	2257	2252	2253 (4)	2257
ν_{11}(e$_g$)	β_{SiH_3}	941	939	906	908	901 (19)	899
			936	904	906	901 (14)	901
ν_{12}(e$_g$)	γ_{SiH_3}	628	626	376	348	444 (0.04)	459
			626	326	307	396 (0.02)	330 (0.5)
β						57 (2)	79, 27 (10)
						51 (1)	65, 26 (11)
σ						74 (28)	78 (55), 56
						61 (24)	52 (45), 40

[a] IR intensities (in km mol^{-1}) of allowed transitions are listed in parentheses. Top (bottom) numbers refer to the MP2 (B3LYP) level. Experimental frequencies are listed in italics. [b] Symmetry given in the D_{3d} point group. [c] Stretch (σ), rock (γ), torsion (τ), deformation (β). [d] From IR and Raman spectra in the gas phase.[38,39,41]

Removal of one electron from the bonding σ_{Si-Si} orbital causes the Si–Si bond to drastically elongate by ΔR = +0.4 Å and the SiSiH bond angle to shrink by $\Delta \theta$ = −12°, while the Si–H bonds slightly contract by Δr = −0.014 Å. These massive structural changes are similar to those predicted at the MP2/6-31G* level[1] and translate directly into the vibrational frequencies and the corresponding IR spectrum. For example, the Si–Si stretch frequency ν_3 is reduced by a factor of 2 from 419 to 212 cm^{-1}. The Si–H stretch fundamentals $\nu_{1/5/7/10}$ increase by 40–94 cm^{-1}, with an average value of 76 cm^{-1}. The SiH$_3$ rocking frequencies ν_9 and ν_{12} are also reduced by a factor of 1.5 and 2, respectively, and the SiH$_3$ torsional frequency drops by 40%. The symmetric and antisymmetric SiH$_3$ umbrella frequencies ν_2 and ν_6 decrease both by about 15%, while the SiH$_3$ deformation frequencies ν_8 and ν_{11} decrease merely by $\sim$4%. Thus, with the exception of the Si–H stretch modes, all frequencies are substantially reduced upon removal of the bonding σ_{Si-Si} electron, indicating that the force constants for SiH$_3$ rocking, deformation, and torsion as well as Si–Si stretching decrease drastically due to a softer potential in the cation ground state. The potential for internal SiH$_3$ rotation of Si$_2$H$_6^+$ is similar to that for neutral Si$_2$H$_6$ (Fig. 5), with the major difference that the barrier at the D_{3h} transition state is lower in the ionic state, V_3 = 285 (233) versus 377 (336) cm^{-1} at the MP2 (B3LYP) level. Significantly, the barrier in the ionic state is still far too large for tunnelling splittings to be resolved at the

current spectral resolution.[41] As the IR spectrum of the D_{3h} transition state is rather similar to that of the D_{3d} global minimum (Fig. 4), the two configurations cannot be distinguished by the current IR spectroscopic experiment. Most frequencies differ by less than 5 cm^{-1}, and – as expected – the largest differences are predicted for the two SiH$_3$ rocking frequencies ν_9 and ν_{12} with 53 and 19 cm^{-1}, respectively. The NBO charge distribution of Si$_2$H$_6$ and Si$_2$H$_6^+$ detailed in Table 1 suggests that the excess charge arising from ionization from the σ_{Si-Si} orbital is indeed fully localized on the Si–Si bond. The resulting charge distribution in the cation ground state at the MP2 (B3LYP) level assigns high positive partial charge to the Si atoms, q_{Si} = +0.99 (+0.82) e, and much smaller negative charges to the H atoms, q_H = −0.16 (−0.11) e.

To estimate the influence of Ar complexation on the properties of Si$_2$H$_6^+$, minima have been searched for on the Si$_2$H$_6^+$–Ar potential using a variety of starting geometries for energy optimization. The only minimum located at both the MP2 and the B3LYP level is the C_{3v} symmetric structure shown in Fig. 1, in which the Ar ligand binds to one of the SiH$_3$ groups of the D_{3d} conformation of Si$_2$H$_6^+$ on the C_3 symmetry axis (Table 1). In this configuration, the Ar atom can interact optimally with the positively charged Si atom collinear with the partially filled and thus electrophilic σ_{Si-Si} orbital. Other starting geometries, in particular those involving H-bonding to

the Si–H protons, did not yield minima. This observation is attributed to the high positive partial charge on the Si atoms, which are the main attractors for the Ar ligands. In addition, no minimum was obtained with a D_{3h} symmetric $Si_2H_6^+$ ion core, indicating that the weak interaction with Ar does not invert the torsional potential. At the MP2 level, the intermolecular bond in $Si_2H_6^+$–Ar is characterized by a Si–Ar bond separation of $R_{Si–Ar} = 2.99$ Å, a dissociation energy of $D_0 = 881$ cm^{-1}, and intermolecular bend and stretch frequencies of $\beta = 57$ and $\sigma = 74$ cm^{-1}, respectively. Ar complexation at this binding site breaks the symmetry between the two SiH$_3$ groups. The Si–Si bond becomes a bit weaker, and there are minor changes in the SiSiH bond angles and Si–H bond lengths of the two non-equivalent SiH$_3$ groups. As expected, the weak interaction with Ar has only little impact on the intramolecular frequencies of $Si_2H_6^+$. Most frequencies change by less than 5 cm^{-1}, and – as expected – the largest differences are predicted for the two SiH$_3$ rocking frequencies ν_9 and ν_{12} with +47 and +68 cm^{-1}, respectively. Although symmetry reduction from D_{3d} to C_{3v} upon Ar complexation has the interesting effect that many more modes of $Si_2H_6^+$ become IR active for $Si_2H_6^+$–Ar, namely the a$_{1g}$ (ν_{1-3}) and e$_g$ (ν_{10-12}) modes, their activation is minor in all cases ($I < 20$ km mol^{-1}) due to the weak perturbation and could not be exploited in the present work to detect more vibrational transitions. However, in principle this tagging technique may be used in the future to detect the IR forbidden transitions of $Si_2H_6^+$, such as the interesting Si–Si stretch mode (ν_3) via tagging spectroscopy. The attractive part of the intermolecular $Si_2H_6^+$–Ar interaction is mainly based upon charge-induced dipole and dispersion forces. The charge on the Ar ligand is predicted to be less than 0.05 e. As dispersion provides a large contribution to the interaction, the B3LYP level predicts much weaker and longer bonds than the MP2 level (428 vs. 881 cm^{-1}, 3.12 vs. 2.99 Å).

Further complexation with a second Ar ligand on the opposite side of $Si_2H_6^+$–Ar on the C_3 axis restores the original D_{3d} symmetry of the monomer cation. The intermolecular bonds in the $n = 2$ complex are slightly weaker than that for $n = 1$ ($D_0 = 815$ vs. 881 cm^{-1}), consistent with the noncooperative three-body induction forces typically observed for solvation of a molecular core ion with neutral nonpolar and inert solvent molecules.[15,22,54–56] These binding energies are compatible with the observed photo-fragmentation behaviour. Transitions **A** and **B** at around 720 and 925 cm^{-1} are observed only in the single Ar loss channel in both IRPD spectra in Fig. 4.

Finally, we reconsider the spectroscopic assignments of the experimental spectra of $Si_2H_6^+$–Ar$_n$ with $n = 1$ and 2 given in Section 3.1 in the light of the computational results. Clearly, the transitions **A** at 725 and 719 cm^{-1} for $n = 1$ and 2 are assigned to the ν_6 fundamental of the $Si_2H_6^+$ moiety in the $Si_2H_6^+$–Ar$_n$ clusters, which are predicted at 715 and 709 cm^{-1}, respectively. The B3LYP calculations predict small incremental redshifts for this transition of –3 and –6 cm^{-1}, and the latter agrees with the measured shift of –6 cm^{-1}. The extrapolated value for the bare $Si_2H_6^+$ ion is thus $\nu_6 = 728$ cm^{-1}, and the derived ionization-induced redshift of $\Delta\nu_6 = -115.5$ cm^{-1} matches the predicted

value, $\Delta\nu_6 = -116$ cm^{-1}. The ν_6 fundamentals in $Si_2H_6^+$–Ar$_n$ with $n = 1$ and 2 give rise to parallel transitions, which are consistent with the narrow rotational band contours observed (12 and 6 cm^{-1}).

The bands **B** at 926 and 925 cm^{-1} for $n = 1$ and 2 are attributed to the ν_8 fundamental of $Si_2H_6^+$–Ar$_n$, with predicted values of 912 and 910 cm^{-1}, respectively. The B3LYP calculations yield incremental redshifts of –1 and –2 cm^{-1}, and the latter agrees with the observed shift of –1 cm^{-1}. The extrapolated experimental value of $\nu_8 = 927$ cm^{-1} for the isolated $Si_2H_6^+$ ion implies an ionization-induced redshift of $\Delta\nu_8 = -13$ cm^{-1}, which is somewhat smaller than the predicted value of $\Delta\nu_8 = -37$ cm^{-1}. The ν_8 fundamentals in $Si_2H_6^+$–Ar$_n$ with $n = 1$ and 2 give rise to perpendicular transitions, and indeed the observed ν_8 rotational band contours are much broader (25 and 20 cm^{-1} for $n = 1$ and 2) than those of the corresponding parallel ν_6 bands.

The interpretation of bands **C** at 1500 and 1505 cm^{-1} for $n = 1$ and 2 is less certain, as there is no fundamental of the $Si_2H_6^+$ ion with D_{3d} symmetry in this frequency range. Thus, the first option is an assignment to a combination or overtone band. The only possible candidate involving two vibrational quanta is the symmetry-allowed $\nu_6 + \nu_2$ combination (a$_{2u}$) with predicted frequencies of 1502 and 1493 cm^{-1} for $n = 1$ and 2 neglecting cross anharmonicities. A second option is an assignment to a $Si_2H_6^+$ isomer with a connectivity different from the D_{3d} structure. It is possible that higher energy isomers of $Si_2H_6^+$ are also formed in the supersonic plasma expansion, which then could be stabilized and cooled in the adiabatic expansion by collisions and subsequent aggregation with Ar. Indeed, we could identify such a low-energy isomer, namely $H_2SiHSiH_3^+$ with C_s symmetry, which is only 15 (16) kJ mol^{-1} less stable than the D_{3d} structure at the MP2 (B3LYP) level. However, as its predicted IR spectrum is quite different from the observed one (Fig. 6), we exclude at the present stage an assignment to higher energy isomers. The calculated $H_2SiHSiH_3^+$ isomer is characterized by a Si–H–Si bridge with a very long Si–Si contact ($R = 3.04$ Å) and very long Si–H bonds ($r = 1.62$ and 1.66 Å). Thus, the Si–Si stretch frequency is only 135 cm^{-1} and the asymmetric Si–H–Si
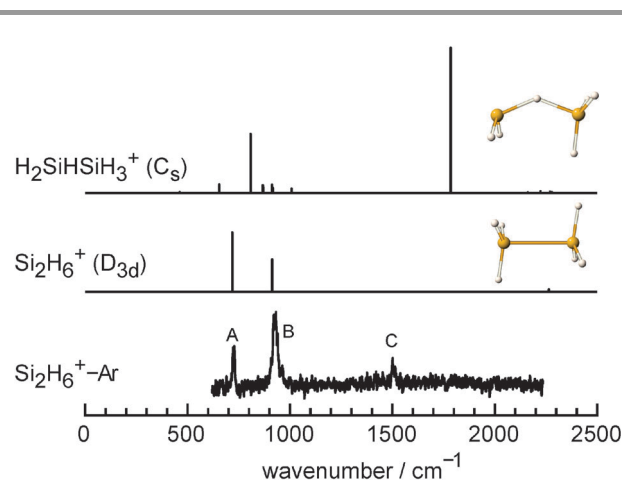

Fig. 6 Experimental IRPD spectra of $Si_2H_6^+$–Ar compared to linear IR absorption spectra of $H_3SiSiH_3^+$ (D_{3d}) and $H_2SiHSiH_3^+$ (C_s) isomers calculated at the B3LYP/aug-cc-pVTZ level.

stretch has also an unusually low frequency (1785 cm^{-1}) and an enormous IR oscillator strength (882 km mol^{-1}). The latter mode is the vibrational IR fingerprint of the Si–H–Si bridge and not observed in the experimental spectra. The third option considered is an assignment to different X$^+$–Ar$_n$ species, which are isobaric to Si$_2$H$_6$$^+$–Ar$_n$ with n = 1 and 2. The CID spectra of the ions with m/z 102 and 142 clearly establish that their composition is of the type 62$^+$-Ar$_{1/2}$ and 102$^+$-Ar (Fig. 3). Possible impurities X$^+$ with m/z 62 are isotopologues of Si$_2$H$_n$$^+$ involving ^{29}Si or ^{30}Si isotopes which occur with natural abundances of 5 and 3%, respectively. Possible candidates for m/z 62 are then ^{28}Si^{29}SiH$_5$$^+$, ^{29}Si$_2H_4$$^+$, ^{30}Si^{28}SiH$_4$$^+$, *etc.* However, we have failed so far to record the IRPD spectra of ^{28}Si$_2$H$_5$$^+$–Ar$_n$ and ^{28}Si$_2$H$_3$$^+$–Ar$_n$, and the IRPD spectrum of ^{28}Si$_2$H$_4$$^+$–Ar also looks different from that of Si$_2$H$_6$$^+$–Ar shown in Fig. 4. Other conceivable impurities X$^+$ with m/z 62 involve species with O atoms such as [SiO$_2$H$_2$]$^+$ due to the presence of H$_2$O impurity in the gas inlet system, as evidenced from the weak (H$_2$O)$_2$$^+$ peak at m/z 36. However, in the presence of oxygen the SiH$_4$ plasma mass spectrum usually exhibits strong signals for SiO$^+$, SiOH$^+$, and SiH$_3$OH$_2$$^+$ at m/z 44, 45, and 49.[36,37] As these ions are completely absent in the mass spectrum in Fig. 2, we also exclude this scenario. In summary, we currently favour the first option with an assignment of bands **C** to $\nu_6 + \nu_2$ of Si$_2$H$_6$$^+$–Ar$_n$.

Inspection of Fig. 4 and Table 2 reveals that, although the Si$_2$H$_6$$^+$ cation has five IR active transitions, only two of them have high IR oscillator strength (ν_6 and ν_8) and are detected in the present experiment. The three other IR active modes have very low IR oscillator strengths ($<$20 km mol^{-1}) and are also outside the investigated frequency range (650–2200 cm^{-1}). Unfortunately, the high IR oscillator strengths of the Si–H stretch fundamentals ν_5 and ν_7 of neutral Si$_2$H$_6$ (120 and 400 km mol^{-1}) are largely quenched upon ionization (1 and 20 km mol^{-1}).

The low-resolution photoelectron spectrum exhibits a progression in the symmetric SiH$_3$ umbrella mode measured to be ν_2(a$_{1g}$) $\sim$ 0.11 eV, which corresponds to $\sim$900 cm^{-1}.[45,46] The current calculations predict for this mode a significantly lower frequency of only $\sim$800 cm^{-1} (817 and 787 cm^{-1} at the MP2 and B3LYP level, respectively). As the vibrational assignment is probably correct and the calculations are accurate to better than $\pm$20 cm^{-1}, the discrepancy is probably due to the large uncertainty in the photoelectron measurement arising from the low spectral resolution.

4. Conclusions

The IR spectrum of the disilane cation, Si$_2$H$_6$$^+$, has been inferred from IRPD spectra of cold Si$_2$H$_6$$^+$–Ar$_n$ complexes (n = 1 and 2). Vibrational analysis guided by MP2 and B3LYP calculations with the aug-cc-pVTZ basis set is consistent with a D_{3d} symmetric structure of H$_3$SiSiH$_3$$^+$ in its ^{2}A$_{1g}$ electronic ground state generated by removal of one electron from the highest occupied bonding σ_{Si-Si} orbital. The only intense IR active fundamentals are the ν_6 and ν_8 modes with frequencies of 728 and 927 cm^{-1}, respectively. The Ar ligands in Si$_2$H$_6$$^+$–Ar and Si$_2H_6$$^+$–Ar$_2$ bind weakly by induction and dispersion forces

at the C_3 rotational axis on opposite sides to the Si$_2$H$_6$$^+$ core ion and cause only little perturbation of its geometric, vibrational, and electronic structure. The calculations reveal a low-energy H$_2$SiHSiH$_3$$^+$ isomer of Si$_2$H$_6$$^+$ with C_s symmetry and a Si–H–Si bridge. Although it is predicted to be only $\sim$15 kJ mol^{-1} less stable than the D_{3d} structure, it is not observed in the experimental spectra. Future efforts are directed toward the vibrational and electronic characterization of related Si$_x$H$_y$$^+$ ions and their complexes to further investigate their intramolecular chemical bonding characteristics and their interaction with solvent molecules.

References

1 L. A. Curtiss, K. Raghavachari, P. W. Deutsch and J. A. Pople, *J. Chem. Phys.*, 1991, **95**, 2433.
2 K. Raghavachari, *J. Chem. Phys.*, 1990, **92**, 452.
3 R. I. Kaiser and Y. Osamura, *Astron. Astrophys.*, 2005, **432**, 559.
4 D. M. Smith, P. M. Martineau and P. B. Davies, *J. Chem. Phys.*, 1992, **96**, 1741.
5 D. W. Boo and Y. T. Lee, *J. Chem. Phys.*, 1995, **103**, 514.
6 Y. B. Cao, J. H. Choi, B. M. Haas, M. S. Johnson and M. Okumura, *J. Phys. Chem.*, 1993, **97**, 5215.
7 W. D. Reents, M. L. Mandich and C. R. C. Wang, *J. Chem. Phys.*, 1992, **97**, 7226.
8 M. C. McCarthy, C. A. Gottlieb and P. Thaddeus, *Mol. Phys.*, 2003, **101**, 697.
9 R. Singh, *J. Phys.: Condens. Matter*, 2008, **20**, 045226.
10 V. Kumar and Y. Kawazoe, *Phys. Rev. Lett.*, 2003, **90**, 055502.
11 M. Okumura, L. I. Yeh, J. D. Myers and Y. T. Lee, *J. Phys. Chem.*, 1990, **94**, 3416.
12 E. J. Bieske and O. Dopfer, *Chem. Rev.*, 2000, **100**, 3963.
13 O. Dopfer, R. V. Olkhov and J. P. Maier, *J. Chem. Phys.*, 2000, **112**, 2176.
14 R. V. Olkhov, S. A. Nizkorodov and O. Dopfer, *J. Chem. Phys.*, 1999, **110**, 9527.
15 R. V. Olkhov, S. A. Nizkorodov and O. Dopfer, *J. Chem. Phys.*, 1998, **108**, 10046.
16 O. Dopfer, R. V. Olkhov, M. Mladenovic and P. Botschwina, *J. Chem. Phys.*, 2004, **121**, 1744.
17 R. A. Relph, J. C. Bopp, J. R. Roscioli and M. A. Johnson, *J. Chem. Phys.*, 2009, **131**, 114305.
18 G. E. Douberly, A. M. Ricks, B. W. Ticknor, W. C. McKee, P. V. R. Schleyer and M. A. Duncan, *J. Phys. Chem. A*, 2008, **112**, 1897.
19 A. M. Ricks, G. E. Douberly, P. V. Schleyer and M. A. Duncan, *J. Chem. Phys.*, 2010, **132**, 051101.
20 P. Botschwina, R. Oswald and O. Dopfer, *Phys. Chem. Chem. Phys.*, 2011, **13**, 14163.
21 D. Roth and O. Dopfer, *Phys. Chem. Chem. Phys.*, 2002, **4**, 4855.

22 O. Dopfer, D. Roth and J. P. Maier, *Int. J. Mass Spectrom.*, 2002, **218**, 281.

23 O. Dopfer, D. Roth and J. P. Maier, *J. Am. Chem. Soc.*, 2002, **124**, 494.

24 G. E. Douberly, A. M. Ricks, P. V. R. Schleyer and M. A. Duncan, *J. Chem. Phys.*, 2008, **128**, 4.

25 R. G. Satink, H. Piest, G. von Helden and G. Meijer, *J. Chem. Phys.*, 1999, **111**, 10750.

26 J. M. Bakker, R. G. Satink, G. von Helden and G. Meijer, *Phys. Chem. Chem. Phys.*, 2002, **4**, 24.

27 A. Fujii, E. Fujimaki, T. Ebata and N. Mikami, *J. Chem. Phys.*, 2000, **112**, 6275.

28 G. E. Douberly, A. M. Ricks, P. V. R. Schleyer and M. A. Duncan, *J. Phys. Chem. A*, 2008, **112**, 4869.

29 A. Patzer, S. Chakraborty, N. Solca and O. Dopfer, *Angew. Chem., Int. Ed.*, 2010, **49**, 10145.

30 N. Solcà and O. Dopfer, *Chem.–Eur. J.*, 2003, **9**, 3154.

31 N. Solcà and O. Dopfer, *Angew. Chem., Int. Ed.*, 2002, **41**, 3628.

32 O. Dopfer, R. V. Olkhov and J. P. Maier, *J. Chem. Phys.*, 1999, **111**, 10754.

33 N. Solcà and O. Dopfer, *J. Phys. Chem. A*, 2003, **107**, 4046.

34 N. Solcà and O. Dopfer, *Chem. Phys. Lett.*, 2001, **347**, 59.

35 A. Patzer, M. Schütz, T. Möller and O. Dopfer, *Angew. Chem., Int. Ed.*, 2012, **51**, 4925.

36 R. V. Olkhov and O. Dopfer, *Chem. Phys. Lett.*, 1999, **314**, 215.

37 R. V. Olkhov, S. A. Nizkorodov and O. Dopfer, *Chem. Phys.*, 1998, **239**, 393.

38 G. W. Bethke and M. K. Wilson, *J. Chem. Phys.*, 1957, **26**, 1107.

39 J. R. Durig and J. S. Church, *J. Chem. Phys.*, 1980, **73**, 4784.

40 N. Moazzen-Ahmadi and V. M. Horneman, *J. Chem. Phys.*, 2006, **124**, 194309.

41 F. Lattanzi, C. Di Lauro and V. M. Horneman, *Mol. Phys.*, 2006, **104**, 1795.

42 B. Beagley, J. M. Freeman, A. R. Conrad, B. G. Norton, G. C. Holywell and J. J. Monaghan, *J. Mol. Struct.*, 1972, **11**, 371.

43 J. V. Ortiz and J. W. Mintmire, *J. Am. Chem. Soc.*, 1988, **110**, 4522.

44 H. Bock, W. Ensslin, F. Feher and R. Freund, *J. Am. Chem. Soc*, 1976, **98**, 668.

45 H. Bock, *Angew. Chem., Int. Ed.*, 1989, **28**, 1627.

46 B. Ruscic and J. Berkowitz, *J. Chem. Phys.*, 1991, **95**, 2407.

47 O. Dopfer, *Int. Rev. Phys. Chem.*, 2003, **22**, 437.

48 O. Dopfer, *Z. Phys. Chem.*, 2005, **219**, 125.

49 M. J. Frisch, G. W. Trucks, H. B. Schlegel, G. E. Scuseria, M. A. Robb, J. R. Cheeseman, G. Scalmani, V. Barone, B. Mennucci, G. A. Petersson, H. Nakatsuji, M. Caricato, X. Li, H. P. Hratchian, A. F. Izmaylov, J. Bloino, G. Zheng, J. L. Sonnenberg, M. Hada, M. Ehara, K. Toyota, R. Fukuda, J. Hasegawa, M. Ishida, T. Nakajima, Y. Honda, O. Kitao, H. Nakai, T. Vreven, J. A. Montgomery Jr., J. E. Peralta, F. Ogliaro, M. Bearpark, J. J. Heyd, E. Brothers, K. N. Kudin, V. N. Staroverov, R. Kobayashi, J. Normand, K. Raghavachari, A. Rendell, J. C. Burant, S. S. Iyengar, J. Tomasi, M. Cossi, N. Rega, N. J. Millam, M. Klene, J. E. Knox, J. B. Cross, V. Bakken, C. Adamo, J. Jaramillo, R. Gomperts, R. E. Stratmann, O. Yazyev, A. J. Austin, R. Cammi, C. Pomelli, J. W. Ochterski, R. L. Martin, K. Morokuma, V. G. Zakrzewski, G. A. Voth, P. Salvador, J. J. Dannenberg, S. Dapprich, A. D. Daniels, Ö. Farkas, J. B. Foresman, J. V. Ortiz, J. Cioslowski and D. J. Fox, *GAUSSIAN09, Rev. A.02*, Gaussian, Inc., Wallingford, CT, 2009.

50 M. D. Halls, J. Velkovski and H. B. Schlegel, *Theor. Chem. Acc.*, 2001, **105**, 413.

51 N. Solcà and O. Dopfer, *J. Am. Chem. Soc.*, 2003, **125**, 1421.

52 N. Solcà and O. Dopfer, *Angew. Chem., Int. Ed.*, 2003, **42**, 1537.

53 S. A. Nizkorodov, Y. Spinelli, E. J. Bieske, J. P. Maier and O. Dopfer, *Chem. Phys. Lett.*, 1997, **265**, 303.

54 R. G. Keesee and A. W. Castleman Jr., *J. Phys. Chem. Ref. Data*, 1986, **15**, 1011.

55 O. Dopfer, *Chem. Phys.*, 2002, **283**, 63.

56 O. Dopfer, *J. Phys. Chem. A*, 2000, **104**, 11693.

This journal is © the Owner Societies 2013

Phys. Chem. Chem. Phys., 2013, **15**, 2774–2781 | **2781**